Thin Solid Films 517 (2008) 909–915

Contents lists available at ScienceDirect

Thin Solid Films

journal homepage: www.elsevier.com/locate/tsf

Luminescence mechanism and carrier dynamic studies of InGaN-based dichromatic light emitting diodes with ultraviolet and blue emissions

Shih-Wei Feng [a,*], Li-Wei Tu [b], Jen-Inn Chyi [c], Hsiang-Chen Wang [d]

[a] Department of Applied Physics, National University of Kaohsiung, No.700, Kaohsiung University Rd., Nan Tzu Dist., 811, Kaohsiung, Taiwan, ROC
[b] Department of Physics, National Sun Yat-Sen University, Kaohsiung, Taiwan, ROC
[c] Department of Electrical Engineering, National Central University, Taoyuan, Taiwan, ROC
[d] Graduate Institute of Opto-Mechatronics, National Chung Cheng University, Chia-Yi, Taiwan, ROC

ARTICLE INFO

Article history:
Received 12 March 2008
Received in revised form 24 August 2008
Accepted 8 September 2008
Available online 14 September 2008

Keywords:
Dichromatic light emitting diodes
Carrier transport
Carrier dynamics
Cathodoluminescence
Time-resolved photoluminescence
Carrier localization
Extraction efficiency
White light emitting diodes

ABSTRACT

In this study, to investigate the luminescence mechanism and carrier dynamics of dichromatic InGaN-based light emitting diodes (LEDs) with two active regions, an ultraviolet (UV)–blue LED (UV active region above the blue one) and a blue–UV LED (blue active region above the UV one) were prepared. Photoluminescence (PL), cathodoluminescence (CL), and time-resolved photoluminescence measurements were performed. For the PL spectra of both LEDs, the blue emissions are stronger than the UV emissions. This trend shows that the higher degree of carrier localization of the blue active region, in either the upper or lower portions of the LEDs, can enhance carrier capture and recombination efficiency. Due to the large and bright light spots emitted from indium-rich clusters in the blue active region, CL images showed that the blue emission is dominant in the image shape for both samples. Furthermore, it was shown that the optical properties and carrier dynamics of dichromatic InGaN-based LEDs could be well explained by the combined effects of the carrier localization effect, structures, extraction efficiency, defect density, and carrier capture efficiency in the UV and blue active regions. Also, thermal effect plays an important role in carrier transport behavior in such dichromatic LEDs. The research results provide important information for operation mechanisms and device designs of dichromatic LEDs.

1. Introduction

White light emitting diodes (LEDs) are one of the candidates for solid-state lighting and liquid crystal displays backlight systems. Using ultraviolet (UV) LEDs to excite red–green–blue phosphors can get better color rendering and power conversion efficiency for generating white light [1]. As the emission wavelength approaches UV, the InGaN-based UV LEDs tend to be inefficient. Due to phase separation and/or indium (In) composition fluctuation in the InGaN quantum wells, blue and green InGaN LEDs show efficient radiative recombination [3–6]. Because of the lower indium composition, a weaker localization effect was proposed to explain the lower external quantum efficiency of UV LEDs [7]. Also, by a comparative study of GaN and InGaN UV (360–380 nm) LEDs, localized states were proposed to as be responsible for the high efficiency of InGaN-based LEDs in spite of a large number of dislocations [8]. On the other hand, because the confinement potential of an UV LED is lower than those found in blue and green LEDs, carrier overflow, particularly in the conduction band, can also lead to a lowered quantum efficiency [9]. Hence, defect density becomes a key issue in the improvement of the light performance of UV LEDs [2,9]. Furthermore, it was demonstrated that dichromatic white light sources are highly efficient for large-screen display, signage, and indicator light applications [2]. The carrier dynamics in dichromatic InGaN LEDs emitting at blue and green spectral ranges were studied by static photoluminescence (PL) and electroluminescence (EL) measurements [2,10]. However, the detailed time-resolved photoluminescence (TRPL) experiment had not been performed to directly examine the carrier dynamics. Understanding the optical properties and carrier dynamics of such dichromatic structures with two active regions is helpful to improve the device performance and to design device structures of white LEDs.

The low miscibility of InN and GaN leads to indium aggregations and phase separations [11]. Spinodal decomposition produced quantum-dot-like structures which formed spatial potential fluctuations and localized energy states for trapping carriers [3–8]. The In-rich InGaN clusters act as quantum dots (QDs) and provide local potential minimums that suppress the diffusion of carriers toward nonradiative defects. It was claimed that the electroluminescence (EL) emissions come from the recombination of localized excitons in In-rich InGaN clusters [12–15]. In our previous study, we proposed the model of carrier transport among different levels of localized states to interpret early-stage fast decay, delayed slow rise, and extended slow decay in the multiple-component decays of PL transient intensity [16]. In

* Corresponding author. Tel.: +886 7 591 9470; fax: +886 7 591 9357.
E-mail address: swfeng@nuk.edu.tw (S.-W. Feng).

0040-6090/$ – see front matter © 2008 Elsevier B.V. All rights reserved.
doi:10.1016/j.tsf.2008.09.032

addition, we have studied the quantum-confinement effect in InGaN quantum cube structures [17]. The calculation results show that the composition, size, and strain of the quantum cube can significantly affect the optical properties.

In this work, to investigate the luminescence mechanism and carrier dynamics of dichromatic InGaN-based LEDs with two active regions, UV–blue LED (UV active region above the blue one) and blue–UV LED (blue active region above the UV one) were prepared. Photoluminescence (PL), cathodoluminescence (CL), and time-resolved photoluminescence (TRPL) measurements were performed. The PL and CL experiment results suggest that the higher degree of carrier localization of the blue active region, in either the upper or lower portions of the LEDs, can enhance carrier capture and recombination efficiency. Furthermore, it was shown that optical properties and carrier dynamics of dichromatic InGaN-based LEDs could be well explained by the combined effects of the carrier localization effect, structures, extraction efficiency, defect density, and carrier capture efficiency in UV and blue active regions. Also, thermal effect plays an important role in carrier transport behavior in such dichromatic LEDs.

This paper is organized as follows: In Section 2, sample structures and experimental procedures are described. In Section 3, experimental results and discussions of UV–blue and blue–UV samples are discussed. Finally, conclusions are drawn in Section 4.

2. Sample structures and experimental procedures

The LED epilayers were grown on *c*-face sapphire substrates in a horizontal low-pressure metal-organic chemical vapor deposition system. Ammonia, trimethylgallium, trimethylaluminum, trimethylidium, biscyclopentadienyl magnesium, and silane were used as precursors and dopants. As shown in Fig. 1, the layer structure of the UV–blue sample consisted of a 25 nm GaN nucleation layer, a 1.5 μm GaN buffer layer, a 1.5 μm *n*-type GaN:Si contact layer, two multiple-quantum-well (MQW) active layers separated by a 5 nm GaN spacer, a 50 nm $Al_{0.1}Ga_{0.9}N$:Mg cladding layer, and a 100 nm *p*-type GaN:Mg contact layer. The UV and blue active regions consisted of five periods $In_{0.06}Ga_{0.94}N$ (3 nm)/GaN:Si (7 nm) and $In_{0.23}Ga_{0.77}N$ (3 nm)/GaN:Si (7 nm) MQWs, respectively. The Si-doping concentration in the barrier layer is around 2×10^{18} cm^{-3}. Also, for the blue–UV LED, blue active region is above the UV one.

Scanning electron microscope (SEM) and CL results were acquired by the use of a Gatan monoCL3 spectrometer in a JEOL JSM 7000F SEM system. The kinetic energies of electrons for CL measurements ranged from 3 to 9 kV with an electron beam current of 60–300 pA. PL measurements were carried out with the 325 nm line of a 50 mW He–Cd laser for excitation. For TRPL measurements, a picosecond diode laser (PicoQuant) generated optical pulses of 100 ps width with a 40 MHz repetition rate to excite the epilayers. The excitation energy was 3.324 eV for pumping the InGaN wells. Light emitted from the sample was detected by a photomultiplier (PMT) and a monochromator. The signal from the PMT was recorded by means of time-correlated single-photon-counting (TCSPC) technology (Model TimeHarp 200, PicoQuant). The overall time resolution was 50 ps. The samples were placed in a cryostat for temperature-dependent measurements.

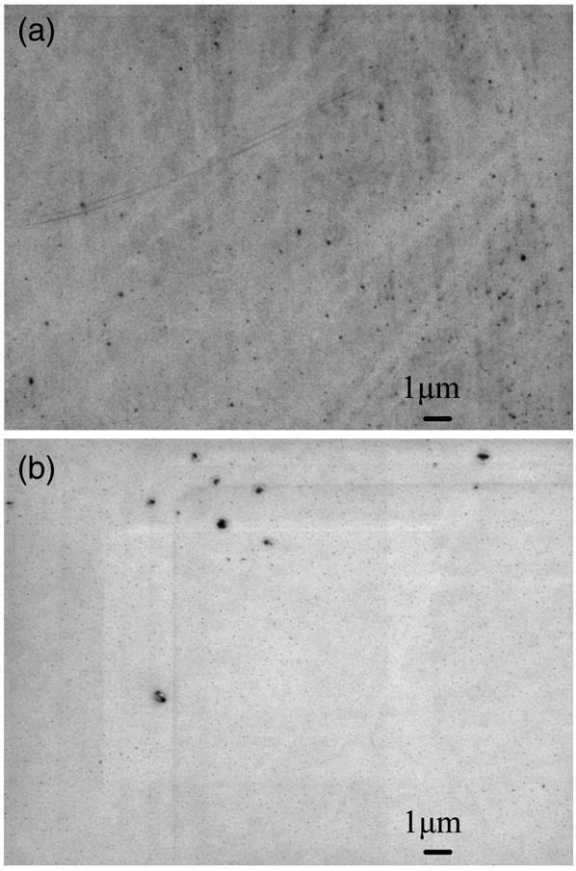

Fig. 2. SEM images of the (a) UV–blue and (b) blue–UV samples.

3. Results and discussions

3.1. SEM results

Fig. 2(a) and (b) shows the SEM images of the UV–blue and blue–UV samples, respectively. A smooth surface morphology and small

UV-Blue LED	Blue-UV LED
p-GaN : Mg contact layer (100 nm)	p-GaN : Mg contact layer (100 nm)
p-$Al_{0.1}Ga_{0.9}N$: Mg cladding layer (50 nm)	p-$Al_{0.1}Ga_{0.9}N$: Mg cladding layer (50 nm)
UV GaN : Si / $In_{0.06}Ga_{0.94}N$ MQWs*5	Blue GaN : Si / $In_{0.23}Ga_{0.77}N$ MQWs *5
GaN : Si spacer (10 nm)	GaN : Si spacer (10 nm)
Blue GaN : Si / $In_{0.23}Ga_{0.77}N$ MQWs *5	UV GaN : Si / $In_{0.06}Ga_{0.94}N$ MQWs*5
n-GaN : Si contact layer (1.5 μm)	n-GaN : Si contact layer (1.5 μm)
GaN buffer layer (1.5 μm)	GaN buffer layer (1.5 μm)
GaN nucleation layer (25 nm)	GaN nucleation layer (25 nm)
Sapphire (0001)	Sapphire (0001)

Fig. 1. Sample structures of the UV–blue (left) and blue–UV (right) LEDs.

dots on the surface were observed in the UV–blue sample. A small dot represents for a defect, beneath which a threading dislocation exists [9]. Both small and larger dots were observed on the surface of the blue–UV sample. From five areas of each sample, the pit densities were estimated to be 1.21×10^8 cm^{-2} and 3.33×10^8 cm^{-2} for the UV–blue and blue–UV samples, respectively. The lower defect density in the UV–blue sample implies that the sample quality of the UV–blue sample is better than that of the blue–UV sample. It was shown that the layer morphology of low-indium-content MQWs was flatter than that of high-indium-content MQWs [11]. Hence, the surface morphology of the UV–blue sample is more uniform than that of the blue–UV sample.

3.2. PL results

Fig. 3 shows the normalized PL spectra of the UV–blue and blue–UV samples at 10 K. In each sample, the PL spectra show both UV and blue emissions. The blue emission in the blue–UV sample is stronger than the UV emission. The followings are the reasons for this result. First, it was claimed that the electroluminescence (EL) emissions come from the recombination of localized excitons in In-rich InGaN clusters [12–15]. With higher indium concentrations, more strongly localized states exist. The higher degree of carrier localization in the blue active region leads to better recombination efficiency. Second, in an ideal LED, when photons are emitted from the active region of the die, they will be subjected to internal reflection [2]. Because of the structures of the LED, the extraction efficiency of the lower active region is relatively smaller. Third, this is partially attributed to the better carrier capture efficiency of the upper active region. Furthermore, in the UV–blue sample, the intensity of the blue emission is also stronger than that of the UV emission. This implies that the higher degree of carrier localization in the blue active region can enhance carrier capture and recombination efficiency. The larger spectrum width of the UV emission than that of blue emission implies a larger interface and/or potential fluctuation. Because of a higher extraction efficiency and better carrier capture efficiency of the upper active region, the UV intensity in the UV–blue sample is stronger than that in the blue–UV sample. Also, a side-bump feature on the long-wavelength side of the blue emission was observed. The existence of the side peaks is attributed to phonon–replica transitions [18].

Fig. 4(a) shows PL peak positions as a function of temperature for the two samples. For both samples, the temperature-dependent PL peak positions of the blue emission show a S-shaped behavior, while those of the UV emission do an unapparent one. The S-shaped behavior has been attributed to the carrier dynamics associated with carrier localization in potential minimums [17]. The lower the indium content in the UV active region, the fewer In-rich clusters. Hence, the apparent S-shaped behavior was not observed in the UV active region. Also, the blue peak positions of the blue–UV sample are red-shifted to

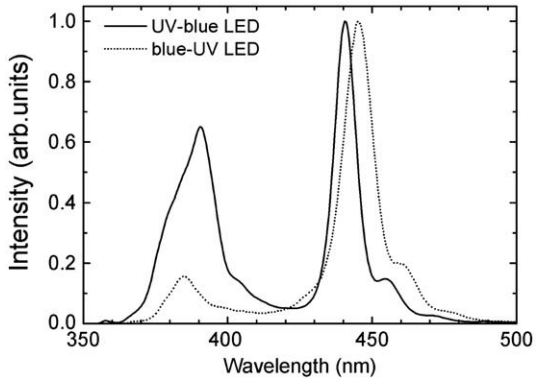

Fig. 3. PL spectra at 12 K of the UV–blue and blue–UV samples.

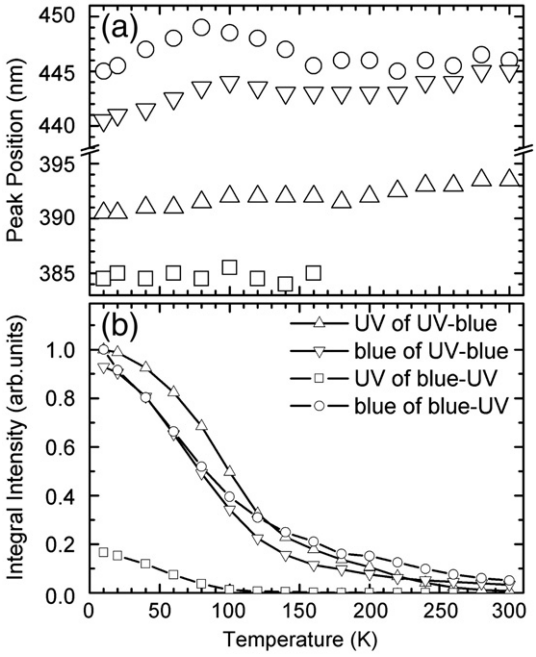

Fig. 4. (a) PL peak positions and (b) integral of the intensities as a function of temperature for the UV and blue emissions of the two samples.

those of the UV–blue sample while the UV peak positions of the blue–UV sample are blue-shifted to those of the UV–blue sample. In previous studies, we have shown that thermal annealing results in In-rich cluster size reduction and the blue-shift of PL peak positions [19]. The peak shifting of the UV and blue emissions can be due to the fact that in growing the upper active region, the high growth temperature conducts a thermal annealing effect on the lower active region. On the other hand, Fig. 4(b) shows the temperature-dependent PL integral intensity of the UV and blue emissions for both samples. The PL integral intensities were normalized at low-temperature (12 K) integral intensities of UV and blue emissions for the UV–blue and blue–UV samples, respectively. As the temperature increased, the enhanced nonradiative recombination decreased the integral intensity. Although the intensity of the blue emission for the UV–blue sample is stronger than that of the UV emission, the integral of the intensity of the UV emission is larger than that of the blue emission. This shows that the upper active region could capture more carriers than the lower one. Furthermore, when the sample temperature was below 120 K, the integral intensity of the UV emission for the UV–blue sample was larger than that of the blue emission for the blue–UV sample. This result is consistent with the lower defect density of the UV–blue sample. At higher temperature(s) (i.e. above 120 K), the integral of the intensity of the UV emission for the UV–blue sample was smaller than that of the blue emission for the blue–UV sample. This phenomenon was due to the less indium composition fluctuation; therefore, the localization effect in the UV active region is weak. With the assistance of thermal energy, carriers can easily escape from the shallow localized states. Such escaped carriers may be trapped by defects such as threading dislocations, thus enhancing nonradiative recombination. Hence, the integral of the intensity of the UV emission for the UV–blue sample becomes smaller than that of the blue emission for the blue–UV sample at higher temperature(s).

3.3. CL results

Fig. 5(a) shows the CL image of the UV–Blue sample with 5 kV electron acceleration voltage excitation, which roughly corresponds to the penetration depth 210 nm. The light spots of a few hundred nanometers in size in the CL image correspond to the indium-rich

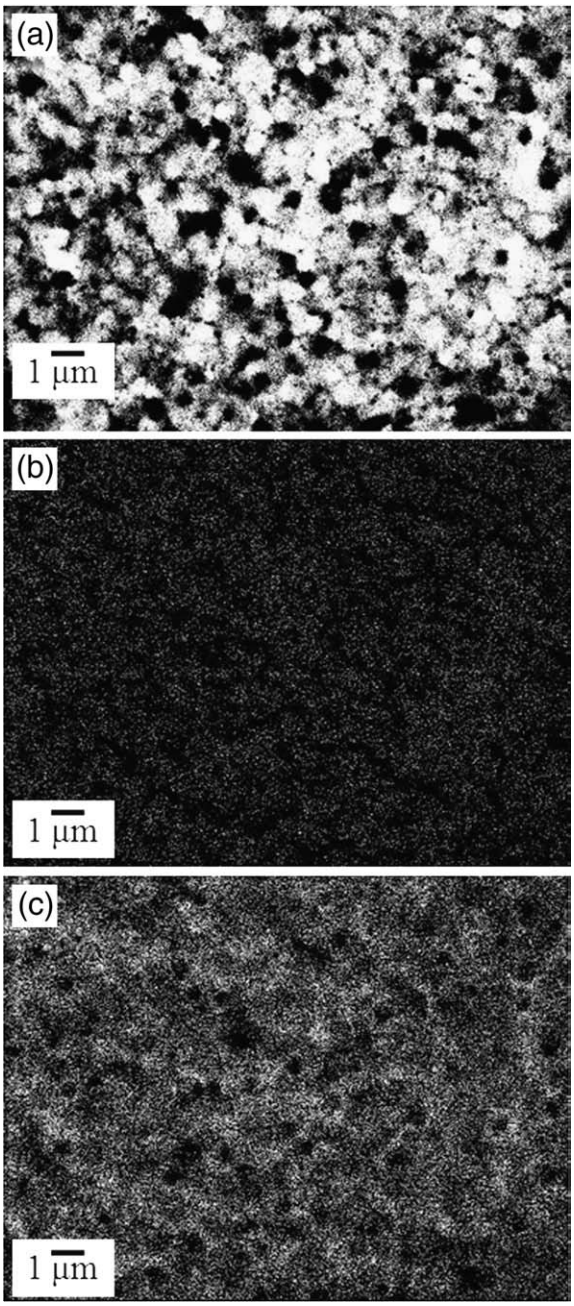

Fig. 5. (a) CL image of the UV–blue sample with 5 kV excitation electron voltage. Monochromatic CL images at the (b) UV and (c) blue peak positions of the UV–blue sample.

clusters [13]. With the excitation of both upper and lower active regions, the light spots emit both UV and blue emissions. This will be shown in Fig. 6 later. Furthermore, the dark regions may represent the defects, which correspond to nonradiative recombination. To analyze the emission property of the image, the CL images were set at the UV and blue peaks in Fig. 5(b) and (c), respectively. It was shown that Fig. 5(a) and (c) look similar while Fig. 5(b) is nearly uniform and featureless. Although the upper active region has a higher extraction efficiency and better carrier capture efficiency, the weaker localization effect in the UV active region makes it harder to enhance recombination efficiency. Hence, the monochromatic CL image for the UV emission shows small and weak light spots. On the other hand, the higher degree of carrier localization in the blue active region can enhance recombination efficiency, so the monochromatic CL image for the blue emission shows larger and brighter light spots. The lower (blue) active region shows larger and brighter light spots while the upper (UV) one emits tiny glimmers. From the top view, the large and bright light spots in the lower active region are more obvious than the small light spots in the upper one. Thus, the images 5(a) and 5(c) are similar while image 5(b) is nearly homogeneous.

On the other hand, Fig. 6(a) shows the CL image of the blue–UV sample with 5 kV excitation. Bright spots and dark regions are also observed in the image. Compared with Fig. 5(a), the higher contrast image implies that the blue emission from the upper active region make major contributions to luminescence. To confirm this argument, we further set the CL image at the blue and UV peak positions in Fig. 6(b) and (c), respectively. One can see that Fig. 6(a) and (b) are similar. Due to the device structures, the upper (blue) active region shows larger and brighter light spots while the lower (UV) one emits tiny glimmers. In the

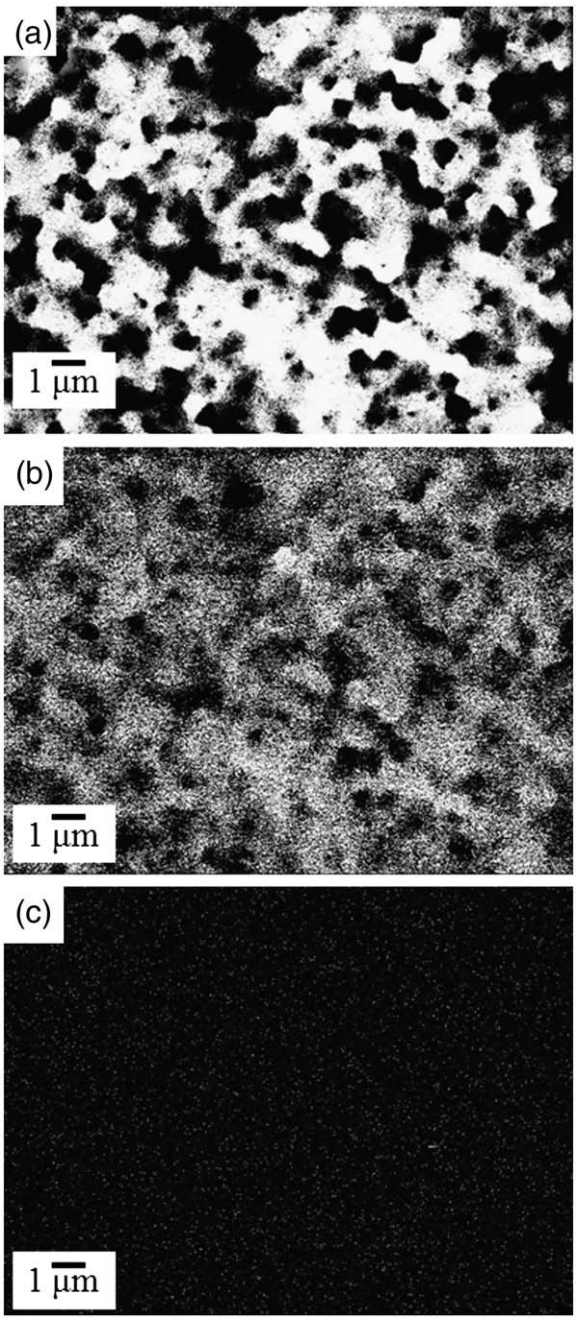

Fig. 6. (a) CL image of the blue–UV sample with 5 kV excitation electron voltage. Monochromatic CL images at the (b) blue and (c) UV peak positions of the blue–UV sample.

top view, the large light spots in the upper portion are brighter than the small light spots in the lower one. Hence, Fig. 6(a) and (b) look similar while Fig. 6(c) looks different. Moreover, due to the LED structures, the lower (UV) active region shows lower extraction efficiency and poorer carrier capture efficiency. The lower In content leads to weaker carrier localization effect. These factors lead to the featureless CL image at the UV peak and to weak luminescence intensity.

Fig. 7 shows the CL spectra of the (a) UV–blue and (b) blue–UV samples. The 3, 5, 7, and 9 kV roughly correspond to penetration depths 88, 210, 400, and 600 nm, respectively. In the UV–blue sample, the UV emission is stronger than the blue emission in a shallow layer (with 3 kV probe). As the electron acceleration voltage increases to excite deep regions, the UV emission reaches a maximum and the blue emission increases. This shows that the luminescence is dominant from the lower active (blue) region. For the blue–UV sample, the blue emission is strong and the UV emission is relatively weak. This confirms that the blue emission from the upper active region makes major contributions to luminescence.

3.4. Carrier dynamics studies

To study carrier dynamics of dichromatic LEDs, we conducted TRPL measurements. Low-temperature (~12 K) temporal behaviors of PL intensity at several emission wavelengths of the UV–blue and blue–UV samples are shown in Fig. 8(a) and (b), respectively. The temporal profiles can be categorized into two groups: UV (solid lines) and blue (dotted lines) curves. For the UV–blue sample, the PL onsets of UV curves emerge somewhat earlier than those of the blue curves. Compared with the UV curves, a time delay about 100 ps (time interval between two vertical dashed lines) was observed for the blue curves to reach maximum intensity. In an ideal LED, when photons are emitted from the active region of the die, they will be subjected to internal reflection [2]. Because of the LED structures, photons emitted from the lower active region require some time to escape into free space and the extraction efficiency of the lower active region is relatively small. Hence, the luminescence from the upper active region of the LED appears earlier, and the second-excited active region reaches its intensity maximum later than the first-excited one. Furthermore, the decays of the short-wavelength curves in each group are relatively faster in the early stage

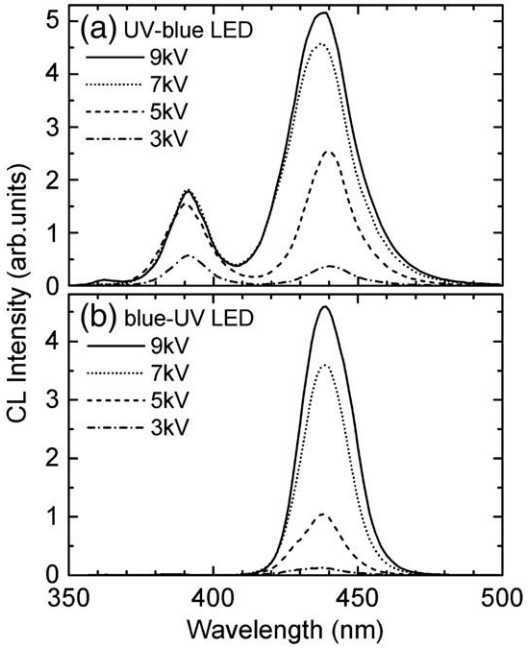

Fig. 7. CL spectra with the excitations of 3, 5, 7, and 9 kV electron voltages of the (a) UV–blue and (b) blue–UV samples at room temperature.

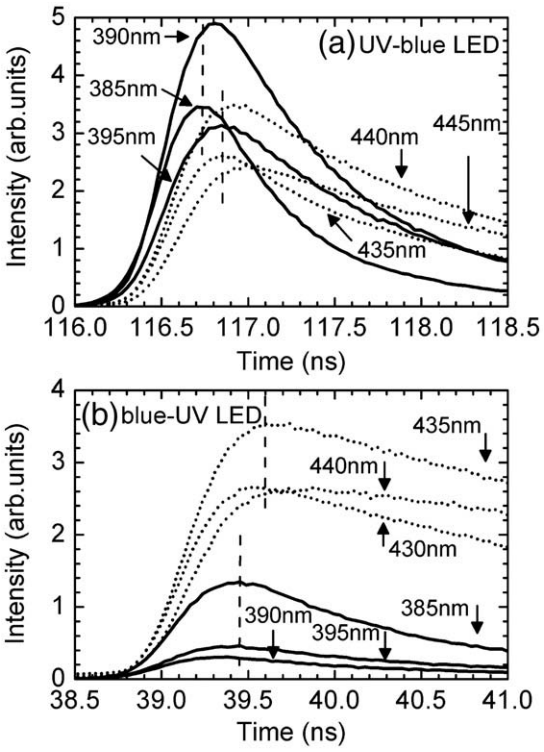

Fig. 8. Low-temperature (12 K) temporal behaviors of PL intensities at several emission wavelengths of the (a) UV–blue and (b) blue–UV samples.

and slower in the extended range. Near the PL spectral peak and on the long-wavelength side, a delayed slow rise for a few hundred picoseconds in the early stage was observed. In the InGaN/GaN system, due to spatial fluctuation of the potential level, carriers may transport among different levels of localized states. It has been proposed that the delayed slow rise was due to the carrier capture process from weaker localized states (higher potential minimums) into stronger ones. Because of fast carrier outflow, the carrier transport process can also be used for interpreting the fast early-stage decay on the high-energy side. In the InGaN-based dichromatic LEDs, a correspondent carrier transport model described in our previous study could also be applied to study the carrier dynamics in both active regions [16].

For the blue–UV sample, the PL onsets of the blue curves emerge somewhat earlier than those of the UV curves. This is also due to lower extraction efficiency and internal reflection of the lower active region. In the blue group, the features, such as early-stage fast decay, delayed slow rise, and extended slow decay, associated with the carrier transport model were also observed [16]. Meanwhile, the UV emission from the lower layer reaches its intensity maximum earlier than the blue emission from the upper layer. Due to the LED structures, the lower (UV) active region shows poorer carrier capture efficiency and lower extraction efficiency. The lower In content leads to weaker localization effect. These factors lead to lower carrier capture efficiency. Hence, less time is needed for fewer carriers to be injected into the lower active region and the rise times of the UV curves were shorter. Also, because of fewer carriers captured in the lower active region, carrier transport into strongly localized states in the lower active region is weak. This leads to the absence of the delayed slow rise feature near the PL spectral peak and on the long-wavelength side in the UV group. Those arguments are consistent with the PL results in Fig. 3.

The decay profiles were fitted with double exponential decays to trace out early-stage (fast) and extended (slow) decay times. Fig. 9 shows the early-stage (filled symbols) and extended (blank symbols) decay times as a function of emission wavelength for the two samples at 12 K. For the UV–blue sample, early-stage decay times at the short-wavelength ends in the UV and blue spectral ranges are shorter than

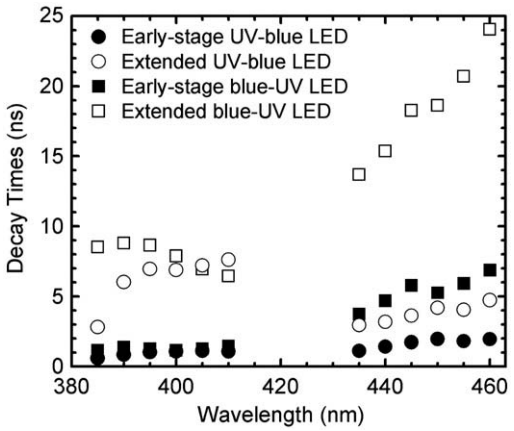

Fig. 9. Wavelength-dependent early-stage (filled symbols) and extended decay times (blank symbols) of the two samples at 12 K.

1 ns. Early-stage decay time increases with increasing emission wavelength for both samples. This is a typical feature of the localized exciton model, whose trap centers originate from a spatial disorder such as the fluctuation of the well width and/or the In composition fluctuation within InGaN/GaN MQWs [16]. Within the localization model, strongly localized (lower-energy) excitons decay primarily via radiative recombination, while weakly localized (higher-energy) excitons exhibit a decreased decay time due to the additional channel of transfer to lower-energy sites. As the emission photon wavelength increases across the PL spectra of the blue–UV sample, the early-stage decay times in the blue spectral range are longer and show an increased slope compared to those in the UV spectral range. Because the larger In composition fluctuation of the blue active region enhanced the localization effect, blue emission is favored by the localized exciton model. For the UV–blue sample, the early-stage decay times in the blue spectral range are also longer and show increased slope compared to those in the UV range as the emission wavelength increases. Although the upper (UV) active region of the UV–blue sample captures more carriers than the lower (blue) one, the longer early-stage decay times in the blue spectral range imply that carrier transport among stronger localized states takes a longer time. Furthermore, in the blue spectral range, the early-stage decay times for the blue–UV LED are longer than those for the UV–blue LED. Under the same excitation condition, the blue active region in the upper part of the blue–UV sample captures more carriers than the lower part of the UV–blue sample. In our previous study, the early-stage decay times were shown to increase in amount with the increased application of excitation power. [16]. As excitation power increases, more carriers are needed to transport the localized states and carrier relaxation therefore takes longer. Hence, the early-stage decay times of the blue–UV sample are longer than those of the UV–blue sample. At the same time, the early-stage decay times in the UV spectral range of the UV–blue sample are slightly shorter than those of the blue–UV one. Although the UV active region on the upper portion of the UV–blue sample captures more carriers than that on the lower portion of the blue–UV sample, the shorter early-stage decay times in the UV range of implies that a better carrier transport efficiency and recombination efficiency. This is consistent with the lower defect density in the UV–blue sample.

For the UV–blue sample, the extended decay times of the UV emissions are longer than those of the blue emissions. Because the upper active region captures more carriers than the lower one, the upper active region needs more time for carrier recombination. The argument can also explain the fact that the extended decay times of blue emissions are longer than those of UV emissions in the blue–UV sample. Furthermore, except in the UV range of the blue–UV sample, the extended decay times show an increasing trend with increasing wavelength. The trend is also due to carrier transport among different localized states [16]. For the blue–UV sample, the extended decay times in the UV range decrease with increasing emission wavelength. Due to a stronger localized effect, higher extraction efficiency, and better carrier capture efficiency of the upper active region, carrier capture of localized states in the lower active region is weak. This results in the decreasing trend. The argument is consistent with the absence of the delayed slow rise feature of the UV group in Fig. 8(b).

To investigate the thermal effect on carrier dynamics, we conducted temperature-dependent TRPL measurements. Fig. 10(a) shows the temperature-dependent early-stage and extended decay times for UV and blue peak positions of the UV–blue sample. A small increase in the early-stage decay times for UV emissions was observed at low temperatures (10–60 K). This implies that a small thermal energy may be helpful for carrier transport. The decreasing trend at relatively higher temperatures (200–300 K) is due to enhanced nonradiative recombination. Because the blue active region shows higher composition fluctuation, transport among the localized states may take more time. Hence, the early-stage decay times in the blue range are longer than those in the UV range. On the other hand, the extended decay times of the UV emission increase at first, then nearly keep constant as temperature rises. The increasing trend in the low-temperature portion can be attributed to the enhanced carrier transport with a reasonable amount of thermal energy (~10 meV). This is partially due to carrier capture from high-energy states [16]. The nearly temperature-independent extended decay times at higher temperature(s) imply a good sample quality. Furthermore, compared with the UV extended decay times, the extended decay times of the blue emission are shorter and they gradually decrease at higher temperature(s). Because fewer carriers were captured by the lower active region, carrier recombination needs less time. This leads to shorter extended decay times of the blue emission. The decreasing trend at higher temperatures is due to enhanced nonradiative recombination.

Fig. 10(b) shows the temperature-dependent early-stage and extended decay times of blue and UV peak positions for the blue–UV sample. The early-stage decay times for both blue and UV emissions

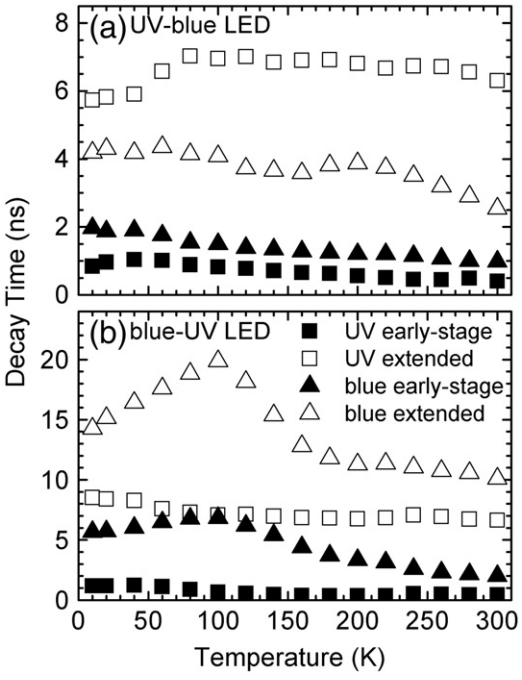

Fig. 10. (a) Early-stage (filled symbols) and extended decay times (blank symbols) for the UV and blue emissions of the UV–blue sample as a function of temperature. (b) Early-stage (filled symbols) and extended decay times (blank symbols) for the UV and blue emissions of the blue–UV sample as a function of temperature.

gradually increase at first, then decrease as temperature rises. This trend can also be explained by the enhanced carrier transport process and nonradiative recombination. Because the blue active region has more strongly localized states, nonradiative recombination is less effective for carriers in strongly localized states. Hence, the blue active region has a higher thermal energy level than UV one. On the other hand, the extended decay times of the blue emission increase at first (10–100 K), then decrease as temperature rises (100–300 K). The increasing trend in the low-temperature portion can be attributed to the enhanced carrier transport with a reasonable amount of thermal energy (~10 meV). This is partially due to carrier capture from high-energy states [16]. The decreasing trend was due to enhanced nonradiative recombination. This was consistent with the large spots in the SEM image as shown in Fig. 2(b). Furthermore, the extended decay times of the UV emissions gradually decrease with temperature. The absence of a step rise of extended decay times of the UV emission in the low-temperature range implies that carrier capture in the lower active region is weak. This is possibly due to carrier escape at higher temperature(s).

4. Conclusions

In summary, we have studied the luminescence mechanism and carrier dynamics of dichromatic UV–blue and blue–UV LEDs. The PL and CL experiment results suggest that the higher degree of carrier localization of the blue active region, in either the upper or lower portions of the LEDs, can enhance carrier capture and recombination efficiency. It was shown that the optical properties and carrier dynamics of dichromatic InGaN-based LEDs could be well explained by the combined effects of the carrier localization effect, structures, extraction efficiency, defect density, and carrier capture efficiency in the UV and blue active regions. Also, thermal effect plays an important role in carrier transport behavior in such dichromatic LEDs. The research results provide important information for operation mechanisms and device designs of dichromatic LEDs.

Acknowledgment

This research was supported by the National Science Council, The Republic of China, under grants NSC 95-2112-M-390-005 and NSC 96-2918-I-390-002.

References

[1] S. Nakamura, G. Fasol, The Blue Laser Diode, Springer, Berlin, 1997.
[2] E.F. Schubert, Light-Emitting Diodes, Cambridge, New York, 2003.
[3] S.F. Chichibu, A. Uedono, T. Onuma, B.A. Haskell, A. Chakraborty, T. Koyama, P.T. Feni, S. Keller, S.P. Denbaars, J.S. Speck, U.K. Mishra, S. Nakamura, S. Yamaguchi, S. Kamiyama, H. Amano, I. Akasaki, J. Han, T. Sota, Nat. Mater. 5 (2006) 810.
[4] E.S. Jeon, V. Kozlov, Y.K. Song, A. Vertikov, M. Kuball, A.V. Nurmikko, H. Liu, C. Chen, R.S. Kern, C.P. Kuo, M.G. Craford, Appl. Phys. Lett. 69 (1996) 4194.
[5] P. Perlin, V. Iota, B.A. Weinstein, P. Wisniewski, T. Suski, P.G. Eliseev, M. Osinski, Appl. Phys. Lett. 70 (1997) 2993.
[6] Y. Narukawa, Y. Kawakami, M. Funato, S. Fujita, S. Fujita, S. Nakamura, Appl. Phys. Lett. 70 (1997) 981.
[7] I.H. Ho, Appl. Phys. Lett. 69 (1996) 2701.
[8] T. Mukai, S. Nakamura, Jpn. J. Appl. Phys. 38 (1999) 5735.
[9] C.C. Pan, C.M. Lee, J.W. Liu, G.T. Chen, J.I. Chyi, Appl. Phys. Lett. 84 (2004) 5249.
[10] Y.L. Li, Th. Gessmann, E.F. Schubert, J. Appl. Phys. 94 (2003) 2167.
[11] Y.S. Lin, K.J. Ma, C. Hsu, S.W. Feng, Y.C. Cheng, C.C. Liao, C.C. Yang, C.C. Chou, C.M. Lee, J.I. Chyi, Appl. Phys. Lett. 77 (2000) 2988.
[12] Y. Narukawa, Y. Kawakami, S. Fujita, S. Fujita, S. Nakamura, Phys. Rev. B 55 (1997) R1938.
[13] T. Hino, S. Tomiya, T. Miyajima, K. Yanashima, S. Hashimoto, M. Ikeda, Appl. Phys. Lett. 76 (2000) 3421.
[14] S.F. Chichibu, K. Wada, J. Müllhäuser, O. Brandt, K.H. Ploog, T. Mizutani, A. Setoguchi, R. Nakai, M. Sugiyama, H. Nakanishi, K. Korii, T. Deguchi, T. Sota, S. Nakamura, Appl. Phys. Lett. 76 (2000) 1671.
[15] Y. Narukawa, Y. Kawakami, S. Fujita, S. Nakamura, Phys. Rev. B 59 (1999) 10283.
[16] S.W. Feng, Y.C. Cheng, Y.Y. Chung, C.C. Yang, Y.S. Lin, C. Hsu, K.J. Ma, J.I. Chyi, J. Appl. Phys. 92 (2002) 4441.
[17] S.W. Feng, T.Y. Tang, Y.C. Lu, S.J. Liu, E.C. Lin, C.C. Yang, K.J. Ma, C.H. Shen, L.C. Chen, K.H. Kim, J.Y. Lin, H.X. Jiang, J. Appl. Phys. 95 (2004) 5388.
[18] S.W. Feng, C.Y. Tsai, Y.C. Cheng, C.C. Liao, C.C. Yang, Y.S. Lin, K.J. Ma, J.I. Chyi, Opt. Quantum Electron. 34 (2002) 1213.
[19] Y.Y. Chung, S.W. Feng, Y.C. Cheng, C.C. Yang, C.H. Tseng, C. Hsu, Y.S. Lin, K.J. Ma, J.I. Chyi, J. Appl. Phys. 93 (2003) 9693.